

Parameterization of Wind Farms in Climate Models

ANNA C. FITCH

Geophysical Institute, University of Bergen, and Uni Research, Bergen, Norway, and Mesoscale and Microscale Meteorology Division, National Center for Atmospheric Research, Boulder, Colorado

JOSEPH B. OLSON

NOAA/Earth System Research Laboratory, and Cooperative Institute for Research in Environmental Sciences, Boulder, Colorado

JULIE K. LUNDQUIST

Department of Atmospheric and Oceanic Sciences, University of Colorado Boulder, Boulder, and National Renewable Energy Laboratory, Golden, Colorado

(Manuscript received 21 June 2012, in final form 15 January 2013)

ABSTRACT

For assessing the impacts of wind farms on regional climate, wind farms may be represented in climate models by an increase in aerodynamic roughness length. Studies employing this method have found near-surface temperature changes of 1–2 K over wind farm areas. By contrast, mesoscale and large-eddy simulations (LES), which represent wind farms as elevated sinks of momentum, generally showed temperature changes of less than 0.5 K. This study directly compares the two methods of representing wind farms in simulations of a strong diurnal cycle. Nearly the opposite wake structure is seen between the two methods, both during the day and at night. The sensible heat fluxes are generally exaggerated in the enhanced roughness approach, leading to much greater changes in temperature. Frequently, the two methods display the opposite sign in temperature change. Coarse resolution moderates the sensible heat fluxes but does not significantly improve the near-surface temperatures or low-level wind speed deficit. Since wind farm impacts modeled by the elevated momentum sink approach are similar to those seen in observations and from LES, the authors conclude that the increased surface roughness approach is not an appropriate option to represent wind farms or explore their impacts.

1. Introduction

The rapid development of wind farms in many countries has led to questions regarding their impacts on the environment, specifically near-surface changes in temperature and humidity. Many wind farms have been developed on agricultural land, thus having the potential to affect the harvest. Direct observational studies of the impacts of wind farms are difficult because of the three-dimensional and multiscale nature of turbulence from individual turbines and from wind farms as a whole. In addition, it is difficult to design an experiment with appropriate controls for observing the effect of wind farms

on local environments. Therefore, modeling studies have proliferated to extend the few observations available. However, questions remain on how best to parameterize the effects of wind farms and how variable the simulated response may be for different parameterization methods.

Modeling studies using mesoscale numerical weather prediction models (Fitch et al. 2012, 2013; Baidya Roy and Traiteur 2010), more finely resolved large-eddy simulations (Lu and Porte-Agel 2011; Calaf et al. 2010), or analytical models (Emeis and Frandsen 1993; Emeis 2010) have explored how as wind flows through a wind farm, the winds decelerate as kinetic energy (KE) is extracted from the mean flow to produce electrical energy. The deceleration of the flow is accompanied by enhanced turbulence caused by the turbulent mixing of the turbine blades and the wind shear at the edge of the

Corresponding author address: Anna C. Fitch, National Center for Atmospheric Research, P.O. Box 3000, Boulder, CO 80307.
E-mail: fitch@ucar.edu

wind speed deficit (or wake). The wake is generated within the layer of the turbine blades, typically between 40 and 150 m above ground level (AGL) and varies in magnitude and length depending on the wind speed, atmospheric stability, and ambient turbulence. In agreement with observations (Högström et al. 1988; Elliott and Barnard 1990; Magnusson and Smedman 1994; Helmis et al. 1995), Fitch et al. (2013) simulated a wind speed deficit that was larger and extended much farther downstream in stable conditions, relative to unstable conditions; because turbulent mixing that would erode the wake was inhibited during stable conditions. In contrast, in unstable conditions the vigorous ambient turbulent mixing rapidly eroded the momentum deficit, minimizing the influence of wind farms on the ambient flow. Furthermore, the turbulent wakes produced by wind turbines have been shown to impact temperatures within the boundary layer (BL), including near the surface (Baidya Roy et al. 2004; Baidya Roy and Traiteur 2010; Baidya Roy 2011; Fitch et al. 2013). The enhanced turbulent mixing can lead to a warming near the surface in stable (nocturnal) conditions and a cooling in unstable (daytime) conditions. The models in these studies showed that during stable conditions the near-surface temperatures were increased up to 0.5 K on average. During unstable conditions, there was a small cooling at the surface, typically less than 0.25 K. However, observations from Baidya Roy and Traiteur (2010) showed greater cooling of up to 2 K. These results contrasted with the more recent study of Zhou et al. (2012), who found small daytime temperature changes and a warming of up to 0.7 K at night. In the large-eddy simulation (LES) conducted by Lu and Porte-Agel (2011), little temperature change near the surface was found. However, the temperature increased within the rotor area by up to 0.5 K. A decrease in temperature of up to 1 K was seen above the rotor area.

The common aspect of the above modeling studies is that the turbines were modeled with an elevated momentum sink (in both LES and mesoscale modeling studies) and an elevated turbulent kinetic energy (TKE) source (only in the mesoscale modeling studies). This approach parameterizes the extraction of momentum in the portion of the atmosphere that directly interacts with the turbine blades, while the resultant wake and surface impacts are modeled by a combination of the resolved turbulent structures and/or the model physical parameterizations. For this approach, the changes in near-surface meteorological conditions are simulated indirectly.

In contrast, many previous modeling studies (Ivanova and Nadyozhina 2000; Keith et al. 2004; Kirk-Davidoff and Keith 2008; Barrie and Kirk-Davidoff 2010; Wang and Prinn 2010, 2011) used an alternative approach to model the effects of wind farms by enhancing the surface

aerodynamic roughness length, z_0 . This method is very computationally efficient, allowing use in global and regional climate studies. However, the near-surface meteorological conditions are directly modified in an attempt to produce a wind speed deficit comparable to observations. Therefore, the resultant changes in the near-surface meteorology are more or less prescribed and are not a physical response to an elevated perturbation. These studies found peak changes in temperature of 1–2 K over wind farm areas, considerably larger than the changes seen in the mesoscale and LES studies described above.

In atmospheric models, the roughness lengths typically vary as a function of vegetation type, with bare soil–desert–water characterized by $z_0 < 0.01$ m, cropland–grassland–shrubland represented by $0.05 < z_0 < 0.15$ m, and forests–urban areas represented by $z_0 \sim 1$ m (Garratt 1993). To produce a wind speed deficit comparable to observed estimates of wind farm wakes (10%–40%, depending on the meteorological conditions), a z_0 of 1–4 m is necessary (Calaf et al. 2010, 2011). Increases in surface roughness lengths can have a profound impact on the surface fluxes of momentum, heat, and moisture, as suggested by Garratt (1993) and as will be shown in this study.

From a mesoscale (or global) modeling perspective, bulk surface flux algorithms are typically based upon the Monin–Obukhov similarity theory and represent the fluxes in terms of mean quantities at the surface ($z = z_s$) and the first model level ($z = z_1$). The turbulent fluxes of momentum (τ) and sensible heat (H) are calculated from the bulk relations (Garratt 1992)

$$\tau \equiv \rho u_*^2 = \rho C_D U^2 \quad \text{and} \quad (1)$$

$$H \equiv -\rho c_p u_* \theta_* = -\rho c_p C_H U (\theta_1 - \theta_s), \quad (2)$$

where ρ is the air density, c_p is the specific heat capacity at constant pressure, u_* is the friction velocity, θ_* is the temperature scale, U is the horizontal wind speed at z_1 , C_D is the drag coefficient, and C_H is the heat transfer coefficient. The momentum flux at the surface [Eq. (1)] is equivalent to the surface shear stress or drag. The transfer coefficients are represented by

$$C_D = \frac{k^2}{\left[\ln\left(\frac{z_1}{z_0}\right) - \Psi_m\left(\frac{z_1}{L}\right) \right]^2} \quad \text{and} \quad (3)$$

$$C_H = \frac{k^2}{\left[\ln\left(\frac{z_1}{z_0}\right) - \Psi_m\left(\frac{z_1}{L}\right) \right] \left[\ln\left(\frac{z_1}{z_t}\right) - \Psi_h\left(\frac{z_1}{L}\right) \right]}, \quad (4)$$

where k is the von Karman constant ($=0.4$), z_0 is the aerodynamic or momentum roughness height, z_t is the

scalar or thermal roughness height, and Ψ_m and Ψ_h are Monin–Obukhov stability functions, which augment the resistance depending on the stability in the surface layer. The roughness lengths for momentum and heat (z_0 and z_t , respectively) differ owing to the different mechanisms of transfer across the interfacial sublayer for scalars and momentum (Garratt 1993).

The aerodynamic roughness length is important for determining the resistance to the coupling between the lowest level of the model atmosphere (z_1) and the surface. Large z_0 and z_t represent rough surfaces that enhance the mixing in the surface layer, thus increasing the fluxes. This effect is represented in the exchange coefficients [Eqs. (3) and (4)], which have logarithmic expressions in the denominator [$\ln(z_1/z_0)$ and $\ln(z_1/z_t)$] representing the resistance to heat and momentum transfer between the land and atmosphere. The existence of z_1 in these expressions suggests that the surface fluxes will also be sensitive to the height of the lowest model level, especially for models configured with high vertical resolution ($z_1 < 10$ m). Shin et al. (2012) investigate the impact of the lowest model level on the surface fluxes but focus on z_0 more representative of cropland or grassland.

To further complicate the impact of very large z_0 , many parameterizations for z_t are dependent upon z_0 , so a large increase in z_0 will reduce both terms representing the momentum and thermal resistance [left-hand side (LHS) and right-hand side (RHS) terms of the denominator of Eq. (4), respectively], producing a large increase in the surface heat fluxes. For example, many models typically use a simple form for z_t :

$$z_t = z_0/c, \quad (5)$$

where c has been set to e^2 (Garratt 1992), 10 (Braud et al. 1993; Beljaars and Viterbo 1994), and 80 (Hopwood 1995), among others. More elaborate forms have related the ratio z_0/z_t to properties of the flow: for example, the roughness Reynolds number, $Re = u_* z_0/\nu$ (Brutsaert 1982; Zilitinkevich 1995). The form developed by Zilitinkevich (1995) has been commonly used in mesoscale models (e.g., Chen et al. 1997; Chen and Zhang 2009):

$$z_t = z_0 \exp[-kC_{zil}(Re)^{0.5}], \quad (6)$$

where C_{zil} is the Zilitinkevich constant and has varied around 0.1 in the literature (Zilitinkevich 1995; Chen et al. 1997; LeMone et al. 2008; Chen and Zhang 2009). The latter parameterization for z_t will reduce z_t sharply for large u_* , thus countering the decreased resistance produced by the larger z_0 . This impact will be shown to be important for modulating the increased surface fluxes

inherent to the enhanced z_0 method for representing wind farms.

In summary, the enhanced z_0 method used to represent the impacts of wind farms may be sensitive to both 1) the height of the lowest model level and 2) the choice of the thermal roughness length parameterization. These sensitivities are relatively unknown for extremely large z_0 used to represent wind farms and need to be better understood if climate impact studies using this method are undertaken. Most importantly, the overall wake structure and surface fluxes from the enhanced z_0 method need to be directly compared to those from the elevated drag approach, which have already been shown to compare well with LES and observations (Fitch et al. 2012). Only if the results compare well can results from the enhanced z_0 approach be appropriate for guiding wind energy policy.

This manuscript is organized as follows: section 2 presents a brief description of the wind farm parameterization and summarizes the suite of simulations used for comparing the two methods of wind farm representation. Section 3 presents the results, which include 1) comparison of the elevated drag and the enhanced z_0 approaches, 2) the impacts of different z_t formulations, and 3) the influence of vertical resolution. Section 4 summarizes and concludes. The findings in this study are important for understanding the different atmospheric responses to wind farms for various parameterization techniques and which techniques produce results that compare more closely to observations.

2. Experimental method

a. Model configuration

The atmospheric response to a wind farm is greatly dependent on not only the ambient wind speed but also the stratification in the boundary layer (Fitch et al. 2013; Hansen et al. 2012; Barthelmie and Jensen 2010; Jensen 2007). These properties will typically vary greatly over a strong diurnal cycle. To compare the two methods of wind farm representation over a wide range of stability conditions, a well-studied case is chosen that exhibits a strong diurnal cycle in an area characteristic of where large wind farms are deployed. The second model intercomparison case study within the Global Energy and Water Cycle Experiment Atmospheric Boundary Layer Study (GABLS2; Svensson et al. 2011) provides the initial conditions and forcing to simulate the diurnal cycle using a mesoscale numerical weather prediction model, the Advanced Research Weather Research and Forecasting model (ARW-WRF version 3.3.1; Skamarock et al. 2008). It is based on observations collected during the

1999 Cooperative Atmosphere–Surface Exchange Study (CASES-99; Poulos et al. 2002) in October 1999 in a region of the U.S. Midwest (Kansas, United States).

The simulations begin at 1400 LT 22 October 1999 and run for 59 h. The model is initialized with a uniformly flat surface and horizontally uniform profiles of potential temperature, specific humidity, and TKE. The diurnal cycle is forced by a prescribed surface skin temperature and the geostrophic wind forcing is constant over time, with the zonal and meridional components of the wind set to 3 and -9 m s^{-1} , respectively, at all levels. A small amount of subsidence, dependent on height, is introduced after 1600 LT 23 October and is of maximum 0.005 m s^{-1} . An f plane is used with the Coriolis parameter set according to the case location of 37.6°N , 96.7°E . The reader is referred to Svensson et al. (2011) for further details.

The domain configuration and physical parameterizations used in the simulation are the same as in Fitch et al. (2012) and the reader is referred to that paper for full details. A two-way nested grid configuration is employed to ensure minimal interaction with the prescribed lateral boundaries. The coarse and fine grids both have dimensions of 202 points \times 202 points, with 3-km and 1-km horizontal resolution for the coarse and fine grids, respectively. The fine grid is centered inside the coarse grid. In the vertical, the levels are progressively stretched toward the top, with 81 levels in total and 30 levels below 1 km. The model top is at 20 km and a Rayleigh relaxation layer of 5-km depth controls reflection. Open radiative lateral boundary conditions are used on all boundaries of the coarse grid, following the method of Klemp and Wilhelmson (1978). For the fine grid, the boundary conditions are interpolated from the coarse grid at the outermost rows and columns of the fine grid. The time step is 9 and 3 s for the coarse and fine grids, respectively.

The physical parameterizations are configured to isolate the turbulent mixing induced by the wind farm, with only the planetary boundary layer (PBL) and surface layer physics active. There are no clouds present in the case and so the microphysics scheme is turned off. Since the diurnal evolution of the BL is forced by the prescribed surface skin temperature, the radiation scheme is also turned off. The PBL physics is parameterized using the Mellor–Yamada–Nakanishi–Niino (MYNN) model (Nakanishi and Niino 2009).

b. Elevated momentum sink parameterization

For the elevated momentum sink representation of the wind farm, the parameterization described in Fitch et al. (2012) is used. This method represents the influence of wind turbines on the atmosphere by imposing a momentum sink on the mean flow at model levels within

TABLE 1. List of the complete set of simulations performed in this study. The name of each simulation is accompanied by the type of parameterization (elevated drag or enhanced surface roughness), z_0 , z_r , and the height of the lowest model midpoint level, z_1 .

Name	Type	z_0 (m)	z_r (m)	z_1 (m)
NF	—	0.03	$z_0/10$	5
NF_ZIL	—	0.03	Zilitinkevich	5
NF37	—	0.03	$z_0/10$	37
NF_ZIL37	—	0.03	Zilitinkevich	37
WFP	Elevated	0.03	$z_0/10$	5
Z0_GABLS	Surface	2.6	$z_0/10$	5
Z0_CONST	Surface	2.6	0.003	5
Z0_ZIL	Surface	2.6	Zilitinkevich	5
WFP37	Elevated	0.03	$z_0/10$	37
Z0_GABLS37	Surface	2.6	$z_0/10$	37
Z0_ZIL37	Surface	2.6	Zilitinkevich	37

the rotor area. A fraction of the KE extracted produces electricity, and the rest is transformed into TKE. The wind turbine thrust coefficient quantifies the total fraction of KE extracted by the turbines and is a function of the wind speed and turbine type. The fraction of this energy that ultimately generates electricity is given by the power coefficient. Both of these proprietary coefficients are measured by the turbine manufacturer.

A hypothetical wind farm similar in scale to the current largest offshore wind farm in the world, Walney in the United Kingdom (see online at <http://www.dongenergy.com/Walney/>), is chosen for these simulations. The wind farm covers $10 \text{ km} \times 10 \text{ km}$ and consists of 100 turbines, each with a maximum power output of 5 MW and is placed at the center of the fine grid. A typical turbine spacing of eight rotor diameters is used, with one turbine per grid cell. The turbines modeled are based on the thrust and power coefficients of the REpower 5M turbine. These turbines have a hub height of 100 m and a blade diameter of 126 m. The cut-in and cut-out wind speeds, below and above which the turbines do not operate, are 3.5 and 30 m s^{-1} , respectively. Between the cut-in speed and 9 m s^{-1} , the thrust coefficient is a maximum and mostly constant with wind speed. At higher wind speeds, the thrust coefficient falls rapidly, where at 13 m s^{-1} (the maximum wind speed in the simulation) the thrust coefficient is approximately half the value at lower speeds.

c. Description of test simulations

The complete set of test simulations for this study is listed in Table 1 along with their important distinctive characteristics. The first four simulations contain no wind farm parameterization of any kind; therefore, their names begin with “NF.” They were performed only to highlight differences created by the wind farms using consistent model configurations. The next four simulations each

employ a method of representing the effects of wind farms and use the high vertical resolution described in section 2a. The first of this set [wind farm parameterization (WFP)] uses the elevated drag parameterization described in section 2b in combination with the standard configuration of GABLS2, using $z_0 = 0.03$ m and $z_t = z_0/10$. The second simulation, Z0_GABLS, also uses the GABLS2 setup; however, it uses $z_0 = 2.6$ m over the area of the wind farm (10 km \times 10 km) to represent the effects of the wind farm (instead of using the elevated drag parameterization). A roughness length of 2.6 m was chosen to compare with previous studies [e.g., the VH simulation (based on the evergreen forest in the model) of Wang and Prinn (2010)] and represents wind turbines with moderate loading and of a similar size and spacing to that in WFP, according to LES analysis by Calaf et al. (2011). Since increasing z_0 will directly impact z_t and may exaggerate the sensible heat fluxes, a third simulation denoted Z0_CONST was performed, keeping z_t the same as in WFP ($z_t = 0.03/10 = 0.003$ m). Finally, a more elaborate form of z_t was tested (Zilitinkevich 1995) that allows z_t to vary with u_* according to Eq. (6), where C_{zil} is set to 0.1, and is named Z0_ZIL. This form is commonly employed in many numerical models and may help limit the large sensible heat fluxes expected with the enhanced z_0 method. Collectively, this set of simulations employing the enhanced z_0 method will be termed the Z0 cases.

Two more Z0 cases were performed to investigate the impact of coarse vertical resolution commonly employed in climate models. A higher first model midpoint level of 37 m compared with 5 m provides a deeper depth to reduce momentum and heat transfers between the land and atmosphere. Both of these coarse-resolution cases, denoted Z0_GABLS37 and Z0_ZIL37, are the same as their high-resolution counterparts apart from the vertical level configuration. These additional experiments are important because the enhanced z_0 method is most typically employed in coarse-resolution global modeling studies, so understanding the impact of vertical resolution is important to interpret the results of previous studies using this method. Finally, the elevated parameterization was tested with coarse vertical resolution; this experiment is denoted WFP37 and uses the same configuration as WFP, apart from the vertical grid.

3. Results

a. Mean wake structure

The wake structure of the wind farm is expected to vary with atmospheric stability (Fitch et al. 2013; Hansen et al. 2012), so we first compare the mean wind farm wakes simulated with these approaches for daytime convective

conditions (1200–1500 LT) and for nighttime stable conditions (2100–0000 LT) on 24 October.

The mean wake structure produced by WFP during the day is shown in Figs. 1a–c. The relatively weak winds at the height of the rotor area (37–163 m) at this time result in lower power production and a small (0.8 m s^{-1} or 10% at most) reduction in the wind. The wake does not persist far downstream as a result. In addition, the vigorous vertical mixing in the unstable BL keeps the momentum deficit to a minimum (Fig. 1c). The vertical wind profile is relatively uniform with height in the convective BL during the day, and the strongest near-surface winds throughout the diurnal cycle occur at this time. In contrast to WFP, in cases in which the wind farm is parameterized by an increase in surface roughness (Figs. 1d–l), the drag on the flow is a maximum during the day when the near-surface wind is strongest. There is a large ($3\text{--}4 \text{ m s}^{-1}$) reduction in the wind within the farm area, resulting in a long wake downstream. Deceleration of the flow occurs ahead of the wind farm, and acceleration is seen on the flanks of the wake. The increased surface roughness method results in the greatest deceleration close to the ground. Conversely, in WFP the greatest deceleration occurs around hub height (100 m AGL).

The strong vertical mixing in the convective BL ensures the momentum deficit generated within the farm area is spread throughout the depth of the BL (Figs. 1c,f,i,l). In addition, in the Z0 cases a large amount of TKE is generated by shear and buoyancy production within the farm area and is transported in the vertical throughout the depth of the BL (shown in Fig. 3 and discussed in more detail in the following section). The largest amount of TKE is generated in the Z0_GABLS case, with a smaller amount in Z0_CONST and the least in Z0_ZIL. The enhanced TKE production in the Z0 cases results in a great increase in the vertical diffusivity and therefore the degree of momentum transport throughout the BL. The wind speed deficit is mixed into the transition layer overlying the BL in the Z0_GABLS and Z0_CONST cases as a result, leaving a smaller reduction within the farm area since the TKE enhances vertical mixing. The largest reduction in the wind in the farm area is seen in Z0_ZIL, where TKE and vertical mixing are lower.

The nighttime conditions (2100–0000 LT) also reveal differences between the parameterizations. At night, the wind in the rotor area is strongest, and more power is produced as a result in the WFP case. The large amount of KE extracted from the flow produces a long wake at hub height (Fig. 2a), with a maximum reduction in the wind of 3.8 m s^{-1} or 30%. Near the surface at a height of 10 m (Fig. 2b), the wind is accelerated as a result of a favorable pressure gradient and enhanced turbulent mixing within the rotor area, which mixes faster flow

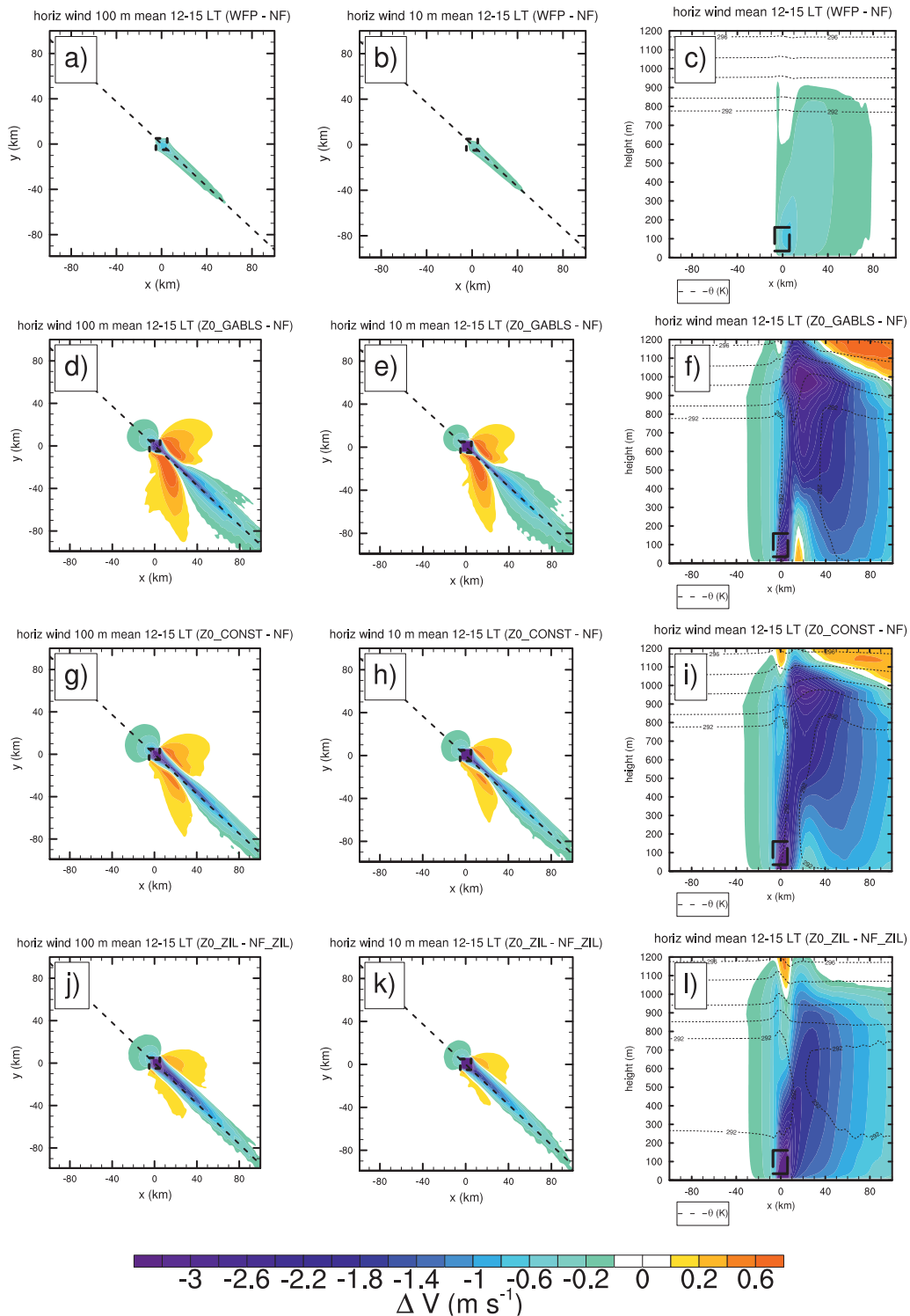


FIG. 1. Horizontal wind speed difference between the wind farm and NF cases during the day: (left) Horizontal cross sections at hub height (100 m), (middle) horizontal cross sections at 10 m, and (right) vertical cross sections along the dashed line in the LHS column. Shown are the (a)–(c) WFP case, (d)–(f) Z0_GABLS case, (g)–(i) Z0_CONST case, and (j)–(l) Z0_ZIL case. Thick dashed lines indicate the wind farm area in the horizontal and the rotor area in WFP in the vertical. Dashed lines in the RHS column indicate potential temperature.

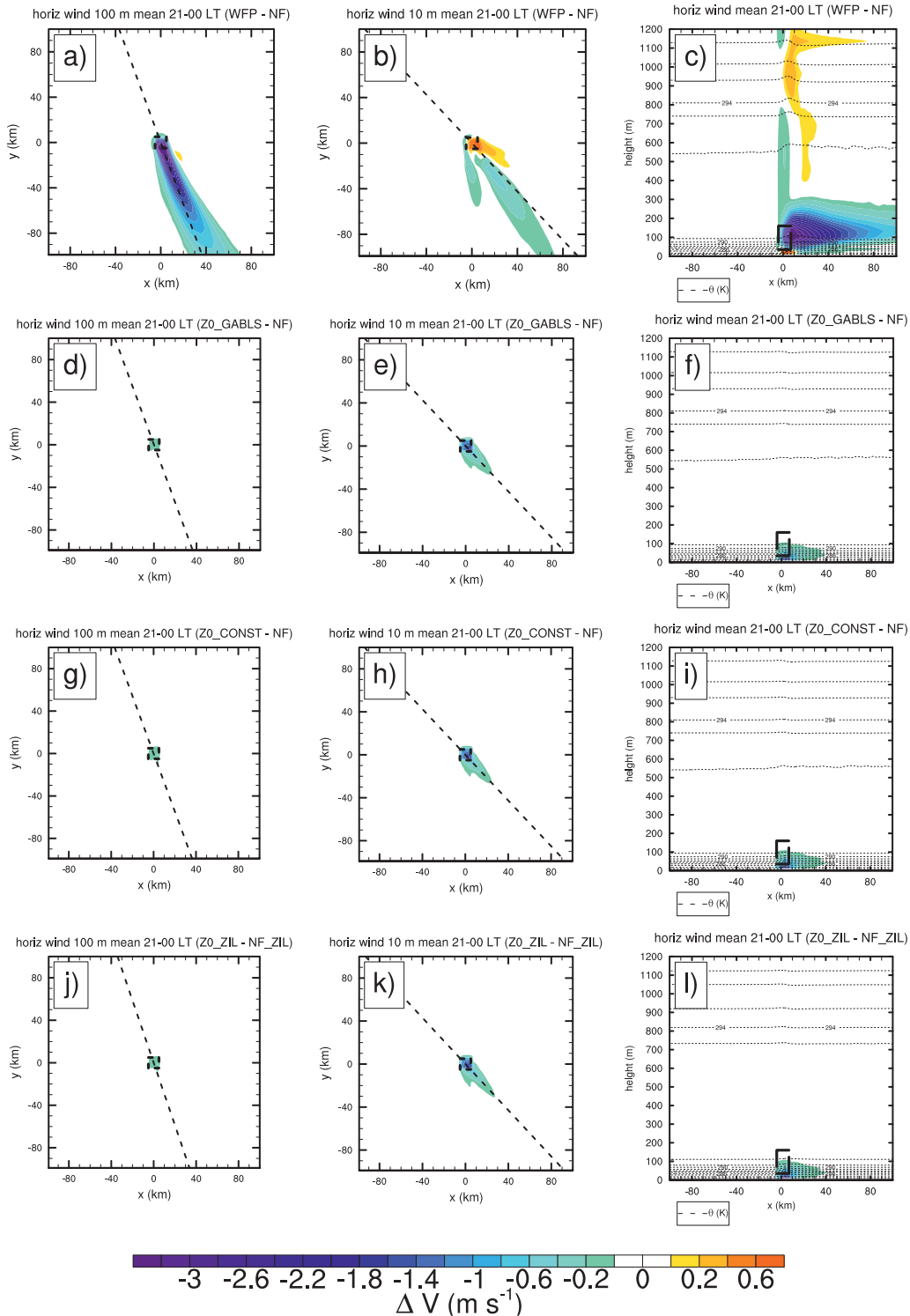


FIG. 2. As in Fig. 1, but for night.

aloft down to lower levels. The enhanced vertical mixing reduces (increases) Ekman turning below (above) hub height, resulting in divergence and convergence on the LHS and RHS of the wake (looking downwind), respectively.

In turn, faster flow aloft is advected down on the LHS of the wake. In the vertical (Fig. 2c), the wake is shallower than during the day because of the inhibition of vertical mixing in the stable layer.

The stable stratification in the BL at night generally causes the wind to weaken considerably near the surface. As a result, in the Z0 cases the surface drag is much reduced compared with during the day, and a very small reduction in the wind, at most 0.2 m s^{-1} , occurs at hub height (Figs. 2d,g,j). No wake is seen beyond the wind farm area in the Z0 cases, contrasting dramatically with the long wake downstream in WFP where a 10% deficit in the wind persists for 60 km downstream. In the Z0 cases, at 10 m (Figs. 2e,h,k) there is a greater reduction in the wind, contrasting with the acceleration seen in WFP. The overall wake structure in the vertical (Figs. 2f,i,l) is much reduced compared with WFP during nighttime stable conditions.

Overall, the WFP and Z0 cases exhibit nearly the opposite wake structure during the day and night. The daytime structures generated using the surface roughness method are not only exaggerated within the wind farm, but also the excessive surface fluxes and production of TKE (analyzed in subsequent sections) transport the deep wind speed deficit into the overlying transition layer. At night, the stable layer near the surface insulates the faster flow aloft from the enhanced surface roughness elements, limiting the size of the wake. In contrast, the elevated drag approach produces only a small wake during the day, while more effectively tapping into the faster flow aloft at night to produce a deep and long wake. The primary reasons for this distinct behavior will be highlighted in the following subsections.

b. Evolution of turbulent kinetic energy

TKE is produced by several mechanisms for each type of wind farm representation and plays a critical role in enhancing the vertical mixing of the wake. In the case of WFP, TKE is produced directly by the parameterization and also indirectly by the PBL scheme through shear production at the top of the rotor area. Below the rotor area, the wind shear is reduced, as is shear production of TKE. In the Z0 cases, TKE is produced primarily by shear production through the increased wind shear generated by the enhanced surface drag. During the day, buoyant production of TKE is also important (although still secondary to shear production) in the Z0 cases (not shown).

Most TKE is produced at night by WFP (Fig. 3a) when winds in the rotor area are strongest. A maximum increase in TKE of $1.0 \text{ m}^2 \text{ s}^{-2}$ occurs in the upper half of the rotor area during the night, an increase by a factor of 20 relative to NF. The increase in turbulent mixing raises the height of the BL above the rotor area. During the day, the wind is weaker in the rotor area, and TKE increases by a maximum of $0.5 \text{ m}^2 \text{ s}^{-2}$ or 33% relative to NF. The increase of TKE in WFP compares well with

the peak TKE production seen in LES in Lu and Porte-Agel (2011), where a maximum of around $0.6 \text{ m}^2 \text{ s}^{-2}$ was observed.

In contrast to WFP, the Z0 cases produce more TKE during the day and very little at night (Figs. 3b–d). More TKE is produced during the day, when the near-surface wind shear is enhanced through greater surface drag, and the large sensible heat fluxes (discussed in section 3d) cause increased buoyancy production of TKE. The TKE is transported throughout the depth of the BL and results in an increase of the BL height with respect to the WFP case. An increase in TKE of up to $20.0 \text{ m}^2 \text{ s}^{-2}$ occurs near the surface in the Z0_GABLS case during the day. The generation of TKE is a factor of 40 greater than that in WFP. At night, the weaker near-surface winds result in lower drag, and much less TKE is produced. The height of the BL is influenced very little as a result for the Z0 cases, in contrast to the WFP case.

As with the reduction in the wind, the generation of TKE in the Z0 cases shows opposite behavior to that in the WFP case. Greatest TKE is always seen near the surface in the Z0 cases, whereas in the WFP case TKE is mostly generated within the rotor area and above. The tremendous increase in TKE during the day in the Z0 cases has not been observed in any modeling or observational studies known (e.g., Mellor and Yamada 1982; Therry and Lacarrere 1983; Nakanishi and Niino 2009). The GABLS2 case (Svensson et al. 2011) shows a maximum in TKE of less than $3 \text{ m}^2 \text{ s}^{-2}$. These results suggest that the large increases in TKE are artifacts of the enhanced z_0 method.

c. Evolution of the vertical temperature perturbation

The enhanced turbulent mixing within the rotor area in WFP induces a temperature perturbation (Fig. 4a) when the BL is stably stratified. Higher θ air is mixed down and lower θ air up, causing a warming (cooling) in the lower half (upper half) of the rotor area during the night. A maximum warming of 1.1 K is seen at the bottom of the rotor area. During the day, little temperature change is seen owing to the well-mixed BL. In their LES, Lu and Porte-Agel (2011) found an increase in temperature within the rotor area of 0.5 K and a cooling above of up to 1 K.

In contrast, in the Z0_GABLS case (Fig. 4b) a strong warming is seen during the daytime, which occurs throughout most of the depth of the BL owing to vigorous vertical mixing in the unstable BL. The positive sensible heat flux during the day (discussed in section 3d) is greatly enhanced in this case, resulting in the warming. A maximum warming of 2.4 K is seen near the ground during the day. At night, the negative sensible heat flux is increased, which causes cooling in the BL by up to 1.5 K.

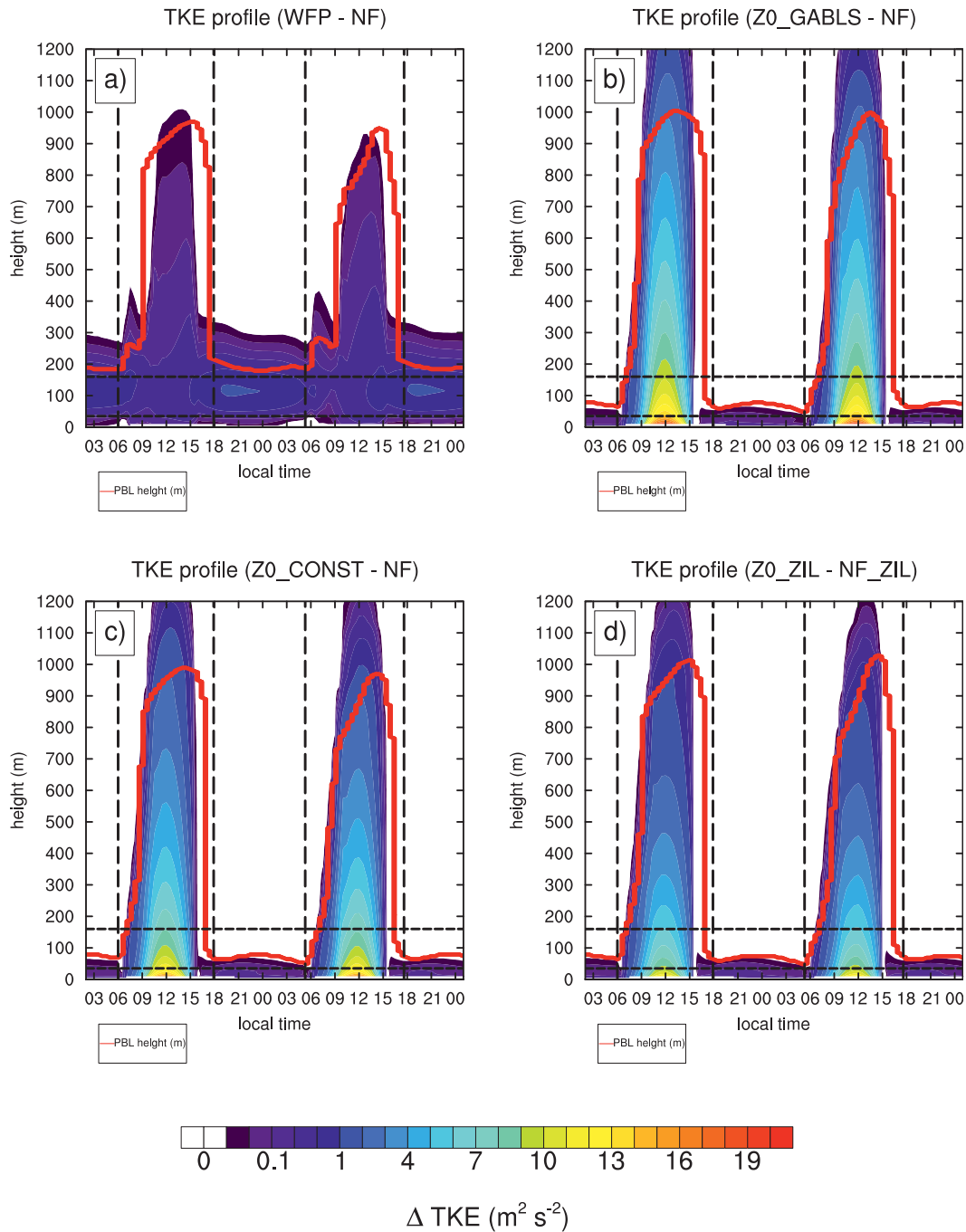


FIG. 3. Evolution of the difference in TKE between the wind farm and NF cases: (a) WFP case, (b) Z0_GABLS case, (c) Z0_CONST case, and (d) Z0_ZIL case. Thick red lines denote the height of the BL in the wind farm case. Vertical dashed lines indicate sunrise and sunset times; horizontal lines indicate the extent of the rotor area in WFP.

The Z0_CONST case (Fig. 4c) shows a similar warming and cooling pattern as Z0_GABLS but with a smaller magnitude of temperature change. A maximum warming of 1.5 K occurs near the surface during the day. At night, slight warming occurs in a very shallow layer close to the ground. The small amount of shear-generated TKE

close to the ground causes mixing of higher θ air down and is enough in this case to overcome the negative sensible heat flux (which is smaller than in the Z0_GABLS case). A maximum warming of 0.2 K occurs near the surface during the night with a cooling above of up to 0.8 K in the rest of the BL. In the Z0_ZIL case (Fig. 4d),

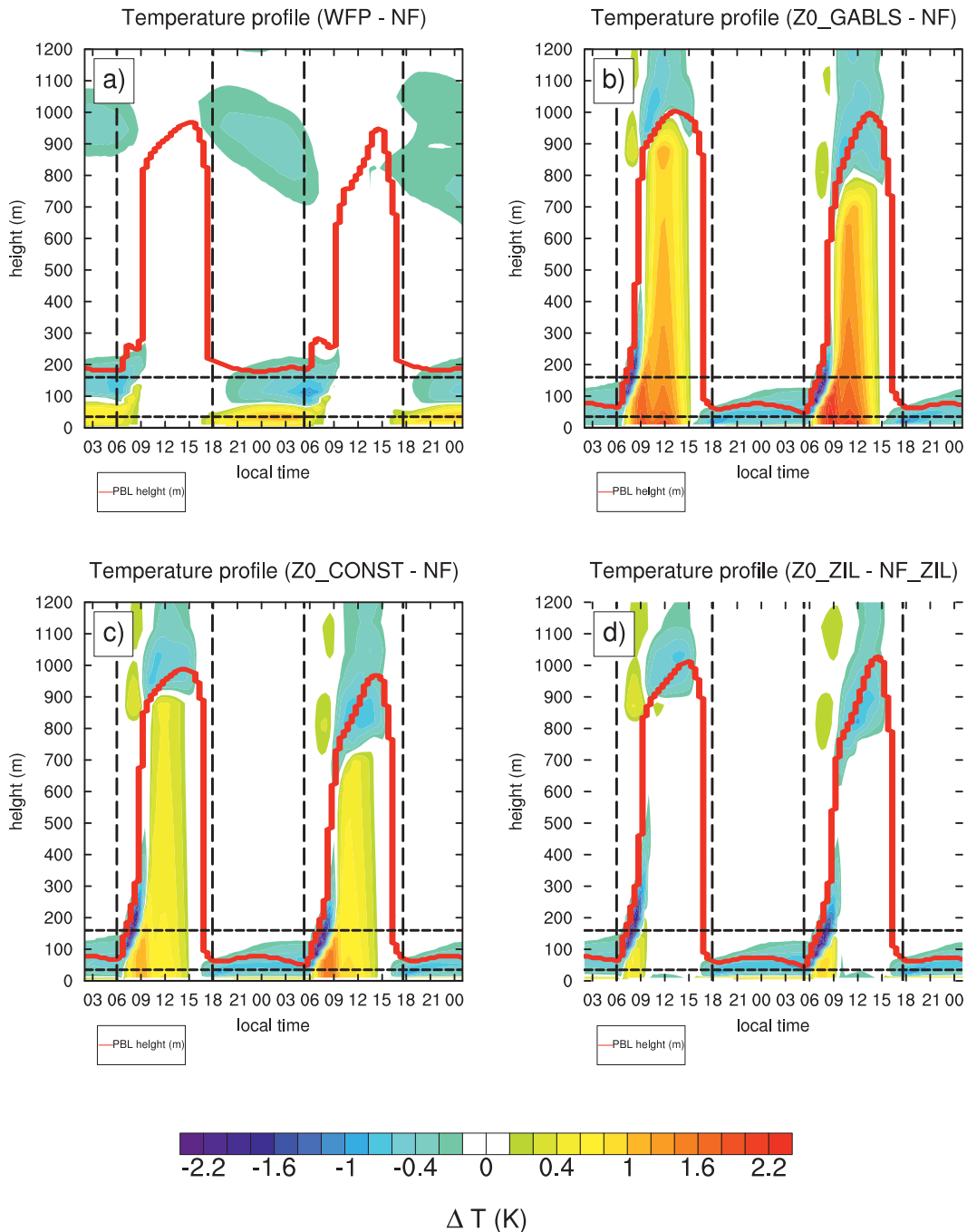


FIG. 4. Evolution of the difference in temperature between the wind farm and NF cases: (a) WFP case, (b) Z0_GABLS case, (c) Z0_CONST case, and (d) Z0_ZIL case. Thick red lines denote the height of the BL in the wind farm case. Vertical dashed lines indicate sunrise and sunset times; horizontal lines indicate the extent of the rotor area in WFP.

the negative sensible heat flux at night is further reduced compared to the other Z0 cases, and a greater warming is seen in the layer closest to the surface by up to 1 K. Above, a similar cooling to the other Z0 cases is observed. During the day, there is a notable absence of warming,

and instead there is very slight cooling near the ground. There is little change in sensible heat flux relative to the no-farm case, and the mixing away of the weak superadiabatic layer in the unstable BL dominates any change in the heat flux.

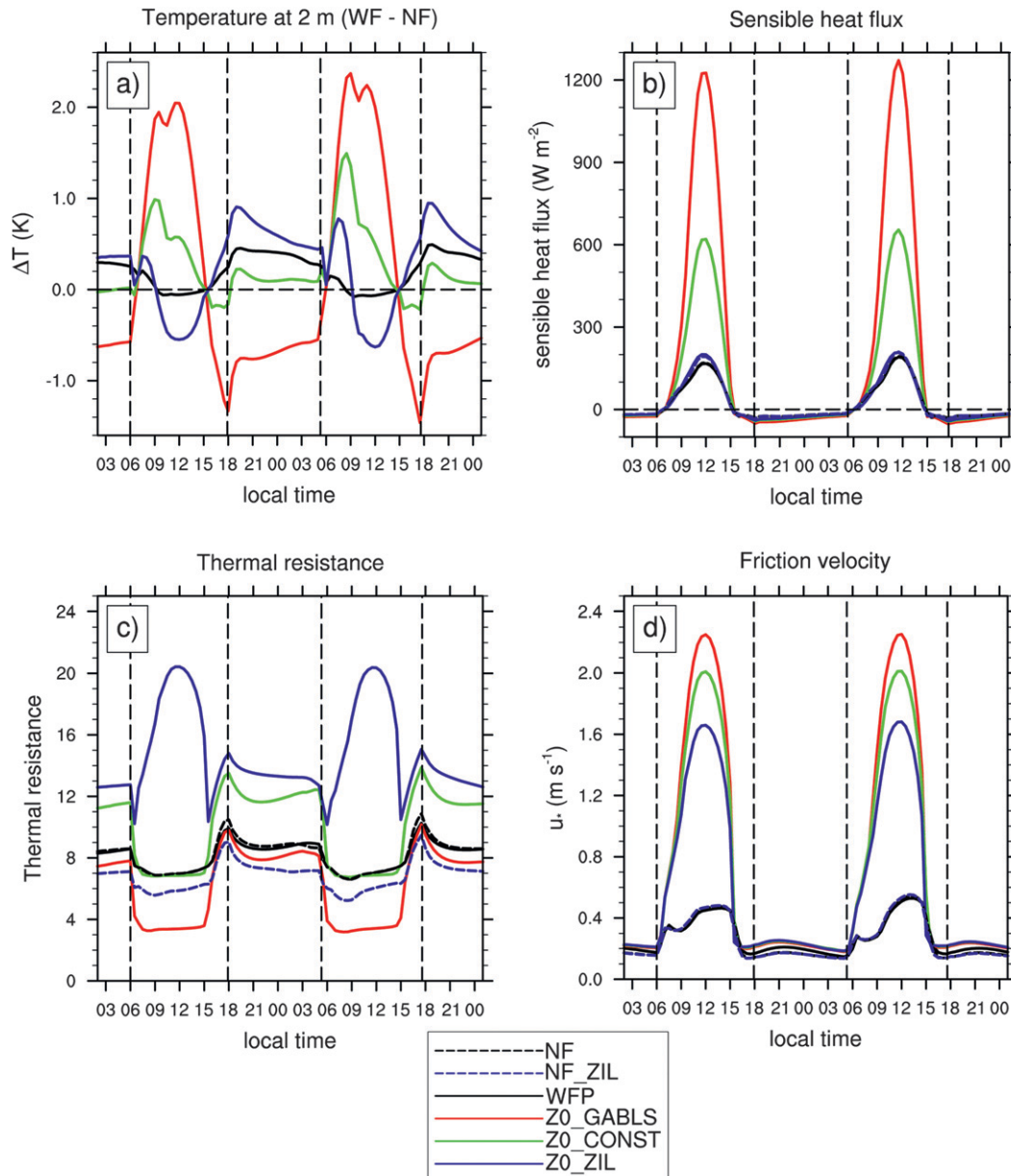


FIG. 5. Evolution over the case of (a) difference in 2-m temperature between the wind farm and NF cases, (b) sensible heat flux, (c) thermal resistance, and (d) friction velocity. Vertical dashed lines indicate sunrise and sunset times.

Overall, the Z0 cases are unable to capture the temperature perturbation induced by the wind farm (WFP) at the correct time or vertical location. The strong daytime warming in the Z0_GABLS and Z0_CONST cases contrasts greatly with the lack of temperature change in WFP during daytime conditions. The Z0_ZIL case is able to capture the correct sign in temperature change near the surface over the diurnal cycle, but the vertical structure and magnitude of the perturbation are still very different compared with the elevated drag approach.

d. Influence on near-surface temperature and heat fluxes

The potential for wind farms to induce near-surface temperature changes has attracted considerable attention. The mean-temperature change over the wind farm (throughout the event) at a height of 2 m in the WFP case is +0.2 K, representing a slight warming (Fig. 5a). A maximum warming of 0.5 K occurs during the night. In the daytime, there is a very slight cooling. These results

compare well with the observations of Zhou et al. (2012), who found small daytime temperature changes and a warming of up to 0.7 K at night. The Z0_GABLS case shows an opposite and exaggerated response to that of WFP, with a strong warming by up to 2.4 K during the day and a cooling by up to 1.5 K at night. The warming observed in Z0_CONST is somewhat moderated, with a maximum increase of 1.5 K in the daytime. In contrast to Z0_GABLS, a slight warming of up to 0.2 K occurs during the night in Z0_CONST. This warming is because vertical mixing dominates over the increased negative sensible heat flux near the surface (discussed in the previous section).

Of the roughness-based wind farm representations, only the Z0_ZIL case exhibits the correct sign in temperature change over the diurnal cycle. However, the warming at night is up to a factor of 2 greater than that in WFP, with a maximum warming of 1 K. During the day, the cooling is up to a factor of 12 greater than WFP, with a maximum decrease in temperature of 0.6 K.

In the simplified physics of the GABLS2 setup, the change in near-surface temperature is the result of two mechanisms: enhanced vertical mixing and changes in the sensible heat flux. In the WFP case, the change in temperature results primarily from enhanced vertical mixing. The change in near-surface temperature then induces a small change in the sensible heat flux (Fig. 5b). In the Z0 cases, the heat fluxes are directly modified through changes in the roughness lengths for heat and momentum [Eq. (2)]. In addition, TKE production through increased wind shear near the surface (and buoyancy production in the day) enhances vertical mixing, such that it can dominate the change in sensible heat flux at night in the Z0_CONST and Z0_ZIL cases.

In the Z0 cases, the sensible heat flux (Fig. 5b) is modified relative to WFP primarily through changes in the roughness lengths for heat and momentum, which appear in the denominator of the heat transfer coefficient equation [Eq. (4)], comprising the full resistance to heating between the land and atmosphere. For convenience, we will label the second term (on the RHS) of the denominator of Eq. (4) the “thermal resistance.” Large thermal roughness lengths (z_t) decrease the thermal resistance and, in turn, increase the heat flux. The thermal roughness length is greatest in Z0_GABLS ($z_t = 0.26$ m), smaller in Z0_CONST ($z_t = 0.003$ m), and smaller still in Z0_ZIL (varies according to u_*). The thermal resistance is thus reduced relative to WFP in Z0_GABLS, resulting in large and unrealistic heat fluxes during the day (Fig. 5b) when the thermal resistance is reduced the most (Fig. 5c). A sensible heat flux of more than 1200 W m^{-2} is seen in Z0_GABLS, whereas the maximum heat flux observed in the GABLS2

case (Svensson et al. 2011) was less than 300 W m^{-2} . In addition, the friction velocity (u_*) is increased by more than a factor of 4 relative to WFP during the day (Fig. 5d), also acting to increase the sensible heat flux. The friction velocity is increased in the Z0 cases through the increase in the roughness length for momentum and also the stronger near-surface winds during the day. At night, the friction velocity is increased only slightly in the Z0 cases relative to WFP since the near-surface winds are weaker at this time.

In the Z0_ZIL case, z_t is a function of u_* [Eq. (6)] and decreases with larger u_* . The decreased z_t acts to increase the thermal resistance, thus offsetting the larger z_0 (which greatly increases u_*). In this case, the large increase in the thermal resistance is enough to reduce the sensible heat flux such that it is similar to WFP.

e. Influence of vertical resolution

The sensible heat flux is sensitive to the height of the first model level above the ground, z_1 , primarily through changes in the heat transfer coefficient [Eq. (4)] and in U [Eq. (2)]. Experiments were performed decreasing the vertical resolution such that the lowest model midpoint level is at 37 m with 21 vertical levels in total, in contrast to the original simulations with 81 vertical levels. The lowest model level height is of the order of that in climate models; the wind farm impact studies of Wang and Prinn (2010) used 18 vertical levels. Two experiments were carried out using lower vertical resolution for the Z0_GABLS and Z0_ZIL cases, denoted Z0_GABLS37 and Z0_ZIL37, respectively. Additionally, corresponding cases with no wind farm present are denoted NF37 and NF_ZIL37, respectively, to enable comparison. The elevated parameterization was tested for its suitability for use with coarse vertical resolution by performing an additional experiment using the same configuration as WFP, apart from the vertical resolution. This experiment is denoted WFP37 and is compared with NF37; in both cases the lowest model midpoint level is at 37 m. In WFP37, there are two model levels within the rotor area.

The reduced u_* in the Z0_GABLS37 and Z0_ZIL37 cases during the day corresponds to reduced surface drag on the atmosphere, leading to a lower reduction in the wind with respect to the high-resolution cases during the day (Figs. 6a,b). At this time, u_* is reduced as the increase in the $\ln(z_1/z_0)$ term in the denominator of Eq. (3) dominates the increase in U with larger z_1 . However, the reduction in the wind is still more than a factor of 2 greater at 100 m than in WFP. In the Z0 cases with high resolution, the deficit in the wind is a factor of 4 to 5 greater than WFP at 100 m. Although the coarse resolution helps to reduce the surface drag, the wind speed reduction during the day is still exaggerated. The WFP37

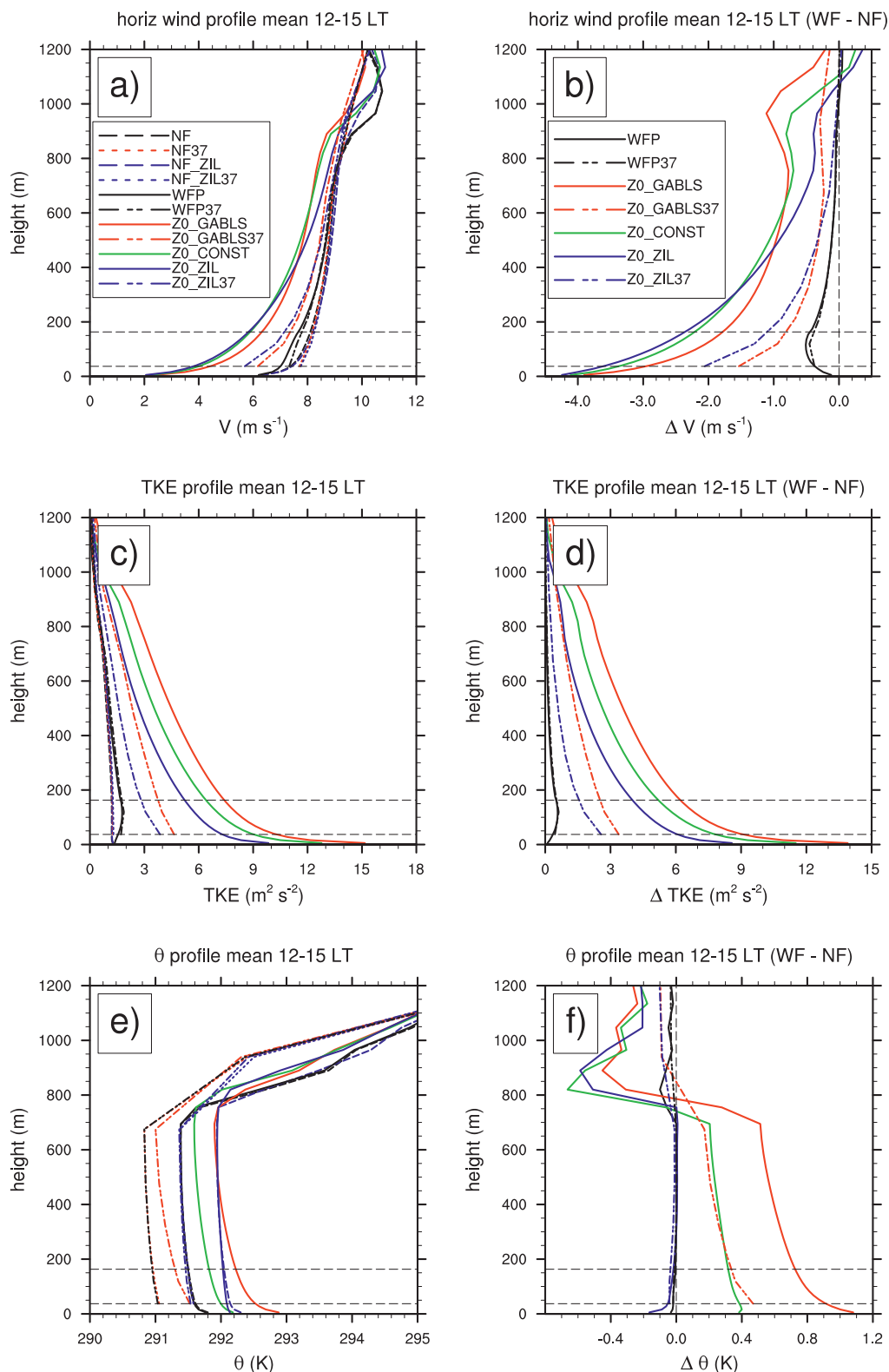


FIG. 6. Mean profiles over the wind farm area during the day: (a) horizontal wind, (b) difference in horizontal wind between the wind farm and NF cases, (c) TKE, (d) difference in TKE between the wind farm and NF cases, (e) potential temperature, and (f) difference in potential temperature between the wind farm and NF cases. Horizontal dashed lines indicate the rotor area in WFP.

case matches very closely the wind reduction seen in WFP, in both magnitude and vertical location. The reduction in the wind in WFP37 is slightly less than in WFP. At night, the reduction in wind at hub height is increased by a factor of 3 to 4 in Z0_GABLS37 and Z0_ZIL37 with respect to the high-resolution cases, owing to the stronger wind at lower levels (Figs. 7a,b). Thus the coarser resolution more closely represents the wind speed deficit in WFP at night but is still too small by a factor of 3 to 4 at hub height. The WFP37 case matches quite closely the wind reduction seen in WFP, with the maximum wind reduction in WFP37 about 16% smaller than WFP. Note that the NF37 and NF_ZIL37 wind profiles are very different from the high-resolution cases (NF and NF_ZIL) during the night, whereas they are similar in the daytime. The assumption that the lowest model level is within the surface layer fails at night in the low-resolution cases, when the height of the BL is approximately 40–50 m. Applying the Monin–Obukhov similarity theory in this case does not obtain an accurate wind profile.

The reduced near-surface wind shear and heat fluxes during the day in the Z0_GABLS37 and Z0_ZIL37 cases are reflected in the TKE profiles (Figs. 6c,d). The lowest-level TKE is reduced by more than a factor of 4 in Z0_GABLS37 and by more than a factor of 3 in Z0_ZIL37, with respect to the high-resolution cases. However, the increase in TKE at hub height is still a factor of 5 and 3 larger in Z0_GABLS37 and Z0_ZIL37, respectively, compared to WFP. The greatest TKE is produced in Z0_GABLS owing to the larger sensible heat flux, followed by Z0_CONST and Z0_ZIL, which have lower heat fluxes. The TKE profile in WFP37 is almost identical to that in WFP. At night, the increased wind shear near the surface in Z0_GABLS37 and Z0_ZIL37 leads to an increase in the TKE relative to the high-resolution Z0 cases (Figs. 7c,d). The amount of TKE produced at hub height is still a factor of 10 smaller than WFP, however. In WFP37, levels with increased TKE match closely with WFP; however, the maximum increase in TKE is reduced by 25%.

The erroneous daytime heating in the BL is reduced by a factor of 2 in Z0_GABLS37 with respect to the counterpart high-resolution case (Figs. 6e,f), due primarily to the reduction in u_* . The overall temperature in the BL is lower in NF37 than in NF because the thermal resistance is greatly increased, lowering the sensible heat flux. Changes in BL temperatures may also be produced by different entrainment rates of warmer air aloft into the BL, as this can occur with changes in vertical resolution. However, studies such as Lenderink and Holtslag (2000) found coarser resolution can increase entrainment, helping to warm the BL. This suggests that the decreased sensible heat fluxes are dominating any

changes in entrainment that may result from coarser vertical resolution. The small decrease in temperature in Z0_ZIL37 is similar to that in Z0_ZIL and is the closest to the temperature change in WFP. Again, the NF_ZIL37 case is cooler overall than NF_ZIL, owing to the larger thermal resistance and lower sensible heat flux. Greatest warming is seen in Z0_GABLS, followed by Z0_CONST, because of the larger heat fluxes. In WFP37, the magnitude and vertical profile of temperature change is almost identical to WFP. At night, the cooling at low levels is reduced by a factor of nearly 2 in Z0_GABLS37 and by a third in Z0_ZIL37, compared with the high-resolution cases (Figs. 7e,f). In WFP37, the vertical profile of temperature change closely follows WFP; however, the maximum warming and cooling is reduced by 60% and 40%, respectively.

Lower resolution reduces the increase in 2-m temperature for Z0_GABLS37 by approximately 0.4 K at most during the day compared with Z0_GABLS (Fig. 8a), owing to the reduced sensible heat flux (Fig. 8b). The lower u_* (Fig. 8d) is primarily responsible for the reduced heat flux. However, the peak warming is the same in both Z0_GABLS37 and Z0_GABLS at 2.4 K during the daytime instead of at night, as occurs in WFP. At night, Z0_GABLS37 shows increased cooling between 1900–0600 LT by up to 0.6 K, an increase by up to a factor of 2. In this case, the decreased thermal resistance (Fig. 8c) relative to Z0_GABLS dominates the small increase in u_* [at this time, the increase in U dominates the increase in the $\ln(z_1/z_0)$ term in the denominator of Eq. (3), giving larger u_*], resulting in a more negative sensible heat flux. The WFP37 case shows similar changes in 2-m temperature to WFP during the day, but at night the warming is very slight. However, it should also be noted that estimates of 2-m temperature are less reliable for coarse vertical resolutions because the 2-m temperature diagnostic can be more heavily tied to the skin temperatures in stable conditions. Therefore, the interpretation of the overall differences in 2-m temperatures may merit caution.

For Z0_ZIL37, the near-surface cooling during the day is modified very little with respect to Z0_ZIL (Fig. 8a). There is a slight increase in the cooling during the morning. During the day, the reduced friction velocity (Fig. 8d) dominates the decrease in thermal resistance (Fig. 8c), resulting in a very slight decrease in the sensible heat flux (Fig. 8b). At night, the peak warming in Z0_ZIL37 at 2 m increases by up to 40% to 1.5 K early in the night but after 0000 LT decreases slightly with respect to Z0_ZIL. The increased TKE in Z0_ZIL37 (Fig. 7d) with respect to Z0_ZIL enhances vertical mixing of higher θ air down, dominating the increase in the negative sensible heat flux during the first

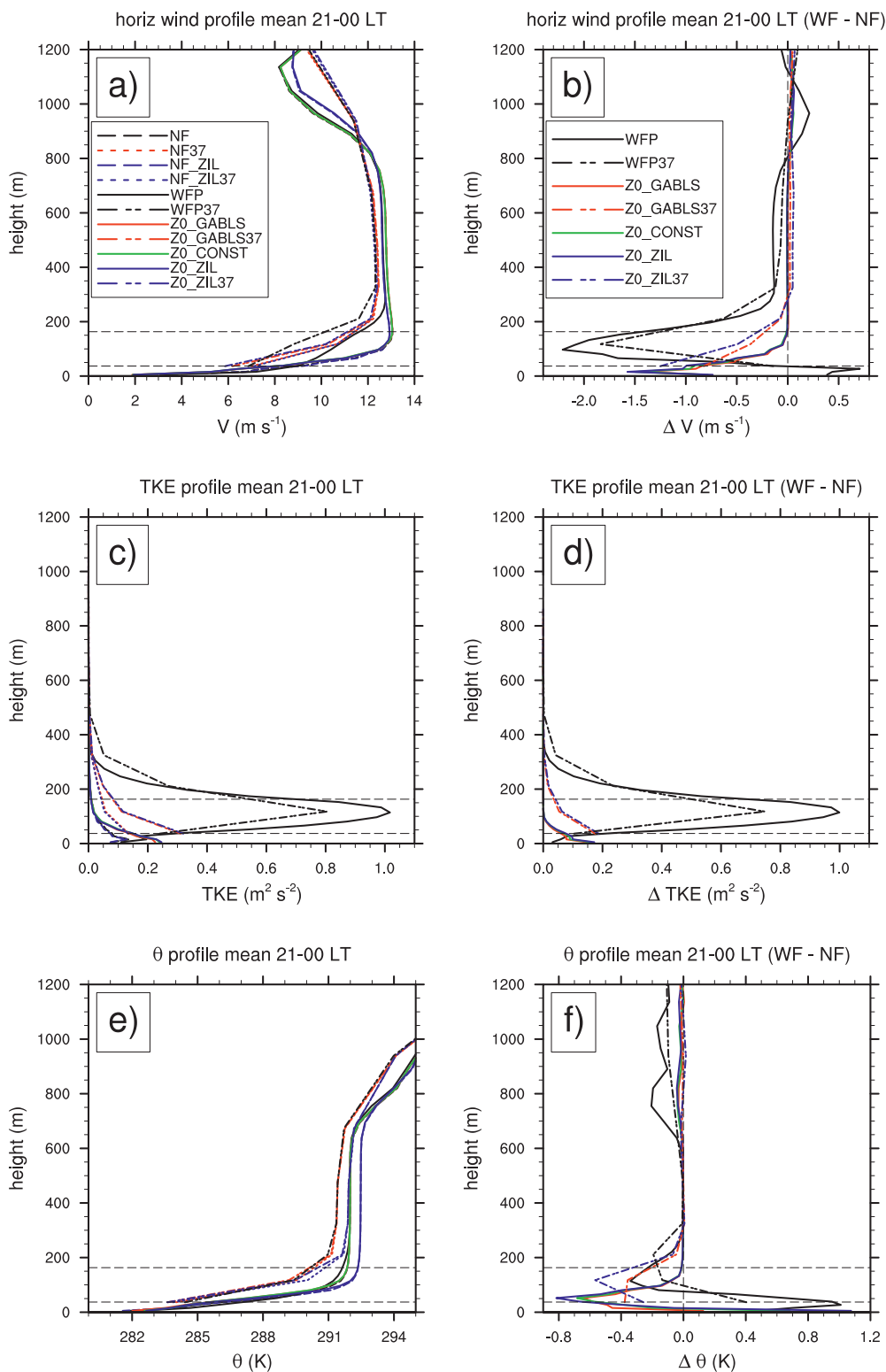


FIG. 7. As in Fig. 6, but for night.

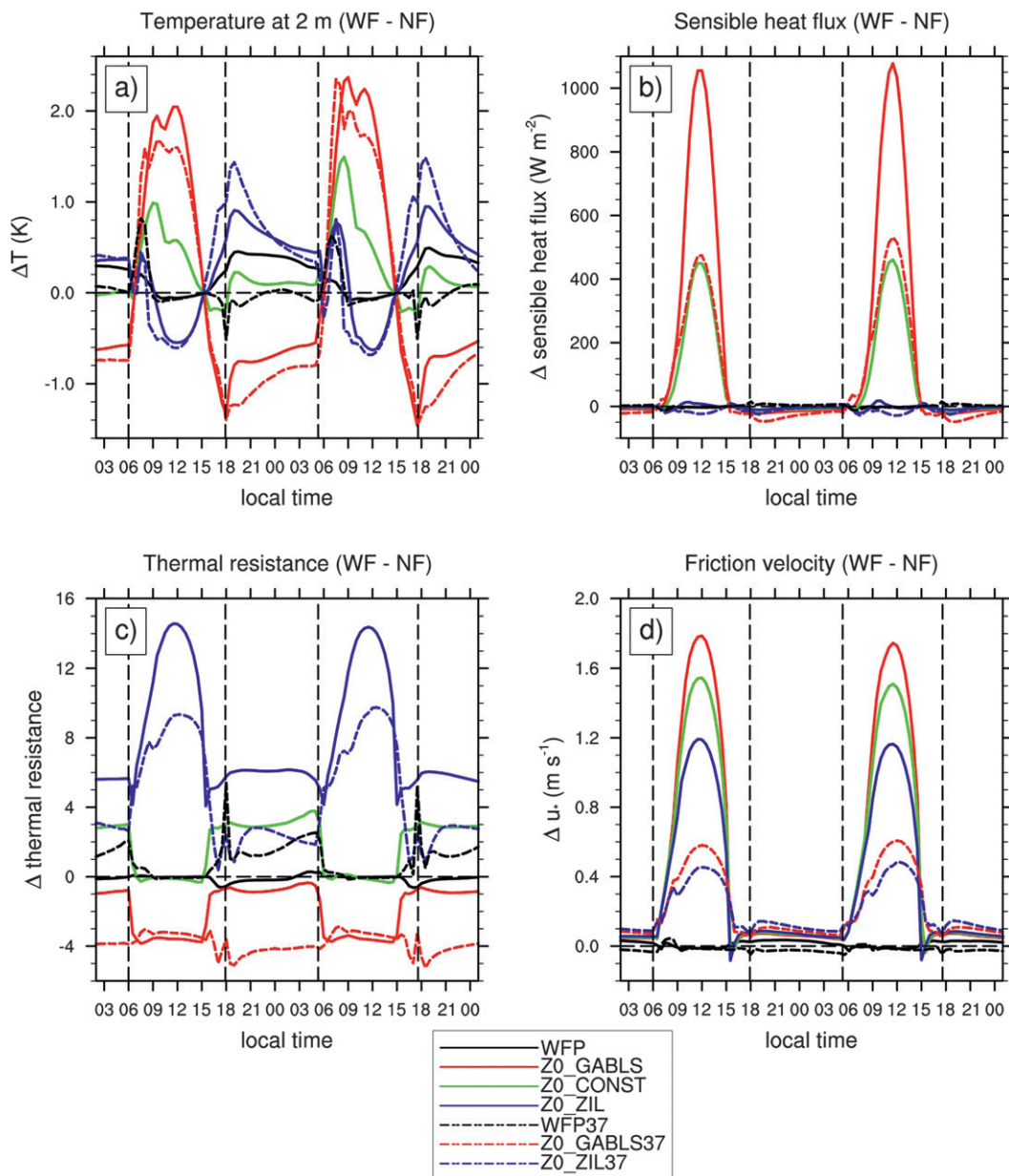


FIG. 8. Evolution over the case of the difference between the wind farm and NF cases of (a) 2-m temperature, (b) sensible heat flux, (c) thermal resistance, and (d) friction velocity. Vertical dashed lines indicate sunrise and sunset times.

half of the night. The relatively warmer 2-m temperature decreases throughout the night and is probably due to the 2-m temperature diagnostic becoming overly coupled to the skin temperature in stable conditions.

Overall, there is a slight improvement in the 2-m temperature during the day with lower resolution in Z0_GABLS37. However, at night the 2-m temperature diverges farther from WFP. The daytime heat flux in Z0_GABLS37 is more reasonable but still too large. Lower resolution in Z0_ZIL37 gives little improvement

and mostly the 2-m temperature diverges farther from WFP, with the peak warming at night increasing. Therefore, the extra resistance gained from the coarser resolution in the Z0 cases results in improved u_* and sensible heat fluxes, but it does not significantly improve the 2-m temperatures or low-level wind speed deficit to be considered a reasonable alternative to the elevated drag approach for representing wind farms. The elevated parameterization performs relatively well with coarse resolution, with profiles of wind reduction, TKE increase, and

temperature change comparing well with the WFP case. However, changes in 2-m temperature follow WFP less closely, with very small temperature changes at night. During the day, the influence on 2-m temperature is very close to that in WFP. Considering that estimates of 2-m temperature are in general less reliable for coarse vertical resolutions, the elevated parameterization performs sufficiently well with coarse vertical resolution that it can be considered more appropriate for representing wind farms in climate models.

4. Discussion and conclusions

The parameterization techniques used to represent wind farms in mesoscale and global models have been compared with specific attention to wind farm impacts on wind speed, turbulence, the resulting wake structure, temperature, and sensible heat flux. Mesoscale models typically represent wind farms as elevated sinks of momentum and sources of turbulence (TKE). In contrast, simulations using global climate models have represented wind farms by increasing the surface aerodynamic roughness length, z_0 , over the area of the wind farm. The large values of z_0 required to represent wind farms (Calaf et al. 2010, 2011) have a profound impact on the surface fluxes of heat and momentum, in turn directly modifying the near-surface meteorology. Studies employing the elevated momentum sink approach have found changes in near-surface temperatures in wind farms to be generally less than 0.5 K, whereas larger impacts with peak temperature changes of 1–2 K were found in studies employing the enhanced z_0 approach. The discrepancy in impacts found by the two different techniques for modeling wind farms warrants further study and the current work is in response to this need.

Simulations were carried out representing a wind farm covering $10 \text{ km} \times 10 \text{ km}$ over land throughout a diurnal cycle. The wind farm was represented by two approaches. In the first, the wind farm was modeled by an elevated momentum sink and source of TKE, as in Fitch et al. (2012, 2013). In the second approach, the wind farm was represented by an increase in the surface aerodynamic roughness length over a $10 \text{ km} \times 10 \text{ km}$ area. A roughness length of 2.6 m was chosen. The sensitivity to different parameterizations for the thermal roughness length, z_t , was also tested. This study is the first to explore these sensitivities when using very large z_0 .

The elevated momentum sink (denoted the WFP case) and enhanced z_0 methods (called the Z0 cases) for representing wind farms exhibit nearly the opposite wake structure, both during the day and at night. The strongest wake in the WFP simulation is observed during the night, with wind speed deficits a factor of 19 greater than the Z0

cases and a wake extending much farther downstream. During the day, the wake is greatly exaggerated in the Z0 cases, with wind speed deficits up to a factor of 5 larger than in WFP. In addition, the Z0 cases exhibit excessive sensible heat fluxes and production of TKE, which transport the deep wind speed deficit into the transition layer above the BL. The large reduction in the wind results in a long wake downstream for the Z0 cases during the day, while WFP exhibits little wake during the day. The greatest reduction in the wind is seen near the surface in the Z0 cases, whereas it is around hub height (100 m AGL) in WFP.

Large and unrealistic sensible heat fluxes are generated during the day in the Z0 cases, where z_t is parameterized as a fraction of z_0 . The large values of both z_t and z_0 reduce the thermal resistance [here defined as the RHS term in the denominator of the expression for the heat transfer coefficient; Eq. (4)], in turn, increasing the sensible heat flux. In addition, the friction velocity (u_*) is greatly increased through the large z_0 and stronger near-surface winds during the day, also acting to enhance the sensible heat flux. In contrast, in WFP only small changes in the sensible heat flux occur through changes in the near-surface temperature. The latter results from enhanced turbulent mixing in the rotor area. In stable conditions, higher θ air is mixed down in WFP, producing warming in the lower half of the rotor area and below, and lower θ air is mixed up, producing cooling in the upper half of the rotor area at night (Fitch et al. 2013). The opposite occurs in daytime convective conditions, with a very slight cooling below the rotor area in WFP.

In the Z0 cases, the enhanced sensible heat fluxes result in warming by up to 2.4 K at 2 m during the day, an opposite and exaggerated response to that of WFP, which shows a very slight cooling. Conversely, at night, a cooling of up to 1.5 K occurs in the Z0 simulations. Again, the opposite is seen in WFP, with a warming of up to 0.5 K. In addition, the Z0 simulations exhibit considerable warming throughout most of the depth of the BL during the day, owing to vigorous vertical mixing in the convective BL. The large sensible heat fluxes and associated temperature changes are somewhat moderated when z_t is set to the same value as in WFP. However, the daytime warming is still greatly exaggerated, with a maximum temperature increase of 1.5 K. During the day, the large sensible heat fluxes, in addition to the enhanced wind shear, generate large amounts of TKE in the Z0 simulations. Near the surface, TKE values of up to $15 \text{ m}^2 \text{ s}^{-2}$ are seen in the Z0 cases, an increase in TKE by up to a factor of 40 relative to WFP. The TKE is transported throughout the depth of the BL, resulting in a great increase in the vertical diffusivity. In turn, the degree of momentum exchange is greatly enhanced, giving rise to large wind

speed deficits throughout the BL. This tremendous increase in TKE has not been observed in any previous modeling or observational studies, suggesting that these features are artifacts of the enhanced z_0 method.

The Zilitinkevich formulation for z_t [Eq. (6)] helps to limit the sensible heat fluxes by reducing z_t for large u_* . This latter approach matched the sensible heat fluxes produced by WFP more closely and was the only method capable of producing the correct sign in near-surface temperature change (to match WFP) throughout the diurnal cycle. However, the magnitude of warming was still up to a factor of 2 greater than WFP, with a maximum warming of 1 K at 2 m. In addition, the daytime cooling was up to a factor of 12 greater than WFP. The mean near-surface temperature change in WFP throughout the case was +0.2 K, a slight warming.

Investigation of the Z0 simulations emphasized that the sensible heat flux is also sensitive to the height of the first model level, z_1 , in addition to the roughness lengths for momentum and heat. Simulations were carried out decreasing the vertical resolution, such that the lowest model level height was increased to 37 m from 5 m. This height is of the order of that used in climate models. The reduced surface drag through the lower u_* during the day resulted in the wind deficit being greatly reduced with respect to the high-resolution cases. However, the reduction in the wind was still up to a factor of 2 greater than in WFP. The reduction in near-surface wind shear results in lower TKE generation, although the amount of TKE is still a factor of 3 to 5 too large. At night, the stronger wind at lower levels results in greater surface drag, but the wind deficit is still too small by a factor of 3 to 4 at hub height compared to WFP. In addition, the enhanced wind shear near the surface gives rise to more TKE generation at night. However, the amount of TKE generated in the coarse Z0 simulations is still a factor of 10 smaller than WFP at hub height.

The excessive heat fluxes during the day are alleviated with lower resolution, with a reduction by a factor of 2 in the sensible heat flux relative to the high-resolution cases. The reduction in u_* is primarily responsible for the lower sensible heat flux. Where z_t is parameterized as a fraction of z_0 , the warming at 2 m is reduced by up to 0.4 K during the day. However, the peak warming remains the same at 2.4 K. At night, the low-resolution case shows increased cooling by up to a factor of 2 relative to the high-resolution case. In this case, the decreased thermal resistance dominates the small increase in u_* , resulting in a more negative sensible heat flux. The low-resolution case, in which z_t follows the Zilitinkevich formulation, shows very little change in cooling at 2 m during the day, relative to the high-resolution case. At night, the peak warming increases by up to 40% to 1.5 K

at 2 m, relative to the high-resolution case. The elevated parameterization is found to perform relatively well with coarse vertical resolution, with wind speed deficits, TKE production, and temperature change comparing well with the high-resolution case. Changes in 2-m temperature compare less well, with very small temperature changes at night. However, it should be noted that estimates of 2-m temperature are less reliable for coarse vertical resolutions because the diagnostic can be more heavily tied to the skin temperatures in stable conditions. Therefore, the interpretation of the overall differences in 2-m temperatures in the coarse-resolution cases may merit caution. Overall, coarse resolution in the Z0 cases results in improved u_* and sensible heat fluxes but does not significantly improve the 2-m temperatures or low-level wind speed deficit.

The changes in temperature observed using the enhanced roughness approach are of a similar magnitude to that reported in previous studies using the same approach (e.g., Keith et al. 2004; Wang and Prinn 2010, 2011), suggesting that our modeling setup and physical parameterizations used are consistent enough to justify the comparison made in this study. The parameterizations of surface momentum and heat fluxes in many other models follow essentially the same approach, using the Monin–Obukhov similarity theory. Thus, the issues highlighted here are likely applicable in other models.

In conclusion, the results presented indicate that modeling wind farms by an increase in surface aerodynamic roughness leads to an atmospheric response that is very different from that found with a more detailed parameterization that allows for elevated drag and generation of TKE. Since the wind farm impacts modeled by the elevated momentum sink approach are similar to those found in LES studies (e.g., Lu and Porte-Agel 2011; Calaf et al. 2010) and wind tunnel experiments reported by Chamorro and Porte-Agel (2009), as well as the few observations available from Christiansen and Hasager (2005) and Zhou et al. (2012), we are led to conclude that the increased surface roughness approach is not an appropriate alternative to represent wind farms. Rather, a direct parameterization of the elevated drag (and source of turbulence) is necessary to produce a realistic wake structure, which then indirectly alters the surface meteorology. The elevated parameterization is found to perform well with the coarse vertical resolution typical of climate models and thus is recommended over the enhanced roughness approach for representing wind farm impacts in global models. However, there is a great need to organize more field campaigns, such as Rajewski et al. (2013), to collect data from large wind farms to further verify the elevated drag approach and improve model parameterizations.

Acknowledgments. We wish to thank REpower for providing the thrust and power coefficients for the 5M turbine. We express our appreciation for research funding from a variety of sources. Funding for ACF is from NORCOWE and support for JKL is from NREL LDRD 06501101. We thank Jimy Dudhia for useful discussions. All the simulations were performed on the NREL/Sandia Red Mesa high-performance computing system. NREL is a national laboratory of the U.S. Department of Energy, Office of Energy Efficiency and Renewable Energy, operated by the Alliance for Sustainable Energy, LLC.

REFERENCES

- Baidya Roy, S., 2011: Simulating impacts of wind farms on local hydrometeorology. *J. Wind Eng. Ind. Aerodyn.*, **99**, 491–498, doi:10.1016/j.jweia.2010.12.013.
- , and J. J. Traiteur, 2010: Impacts of wind farms on surface air temperatures. *Proc. Natl. Acad. Sci. USA*, **107**, 17 899–17 904, doi:10.1073/pnas.1000493107.
- , S. W. Pacala, and R. L. Walko, 2004: Can large wind farms affect local meteorology? *J. Geophys. Res.*, **109**, D19101, doi:10.1029/2004JD004763.
- Barrie, D. B., and D. B. Kirk-Davidoff, 2010: Weather response to a large wind turbine array. *Atmos. Chem. Phys.*, **10**, 769–775, doi:10.5194/acp-10-769-2010.
- Barthelmie, R. J., and L. E. Jensen, 2010: Evaluation of wind farm efficiency and wind turbine wakes at the Nysted offshore wind farm. *Wind Energy*, **13**, 573–586, doi:10.1002/we.408.
- Beljaars, A. C. M., and P. Viterbo, 1994: The sensitivity of winter evaporation to the formulation of aerodynamic resistance in the ECMWF model. *Bound.-Layer Meteor.*, **71**, 135–149, doi:10.1007/BF00709223.
- Braud, I., J. Noilhan, P. Bessemoulin, and P. Mascart, 1993: Bare-ground surface heat and water exchange under dry conditions: Observations and parameterization. *Bound.-Layer Meteor.*, **66**, 173–200, doi:10.1007/BF00705465.
- Brutsaert, W. A., 1982: *Evaporation into the Atmosphere*. Reidel, 299 pp.
- Calaf, M., C. Meneveau, and J. Meyers, 2010: Large eddy simulation study of fully developed wind-turbine array boundary layers. *Phys. Fluids*, **22**, 015110, doi:10.1063/1.3291077.
- , M. B. Parlange, and C. Meneveau, 2011: Large eddy simulation study of scalar transport in fully developed wind-turbine array boundary layers. *Phys. Fluids*, **23**, 126603, doi:10.1063/1.3663376.
- Chamorro, L. P., and F. Porte-Agel, 2009: A wind-tunnel investigation of wind-turbine wakes: Boundary-layer turbulence effects. *Bound.-Layer Meteor.*, **132**, 129–149, doi:10.1007/s10546-009-9380-8.
- Chen, F., and Y. Zhang, 2009: On the coupling strength between the land surface and the atmosphere: From viewpoint of surface exchange coefficients. *Geophys. Res. Lett.*, **36**, L10404, doi:10.1029/2009GL037980.
- , Z. Janjic, and K. Mitchell, 1997: Impact of atmospheric surface-layer parameterizations in the new land-surface scheme of the NCEP mesoscale Eta model. *Bound.-Layer Meteor.*, **185**, 391–421, doi:10.1023/A:1000531001463.
- Christiansen, M. B., and C. B. Hasager, 2005: Wake effects of large offshore wind farms identified from satellite SAR. *Remote Sens. Environ.*, **98**, 251–268, doi:10.1016/j.rse.2005.07.009.
- Elliott, D. L., and J. C. Barnard, 1990: Observations of wind turbine wakes and surface roughness effects on wind flow variability. *Sol. Energy*, **45**, 265–283, doi:10.1016/0038-092X(90)90012-2.
- Emeis, S., 2010: A simple analytical wind park model considering atmospheric stability. *Wind Energy*, **13**, 459–469, doi:10.1002/we.367.
- , and S. Frandsen, 1993: Reduction of horizontal wind speed in a boundary layer with obstacles. *Bound.-Layer Meteor.*, **64**, 297–305, doi:10.1007/BF00708968.
- Fitch, A. C., J. B. Olson, J. K. Lundquist, J. Dudhia, A. K. Gupta, J. Michalakes, and I. Barstad, 2012: Local and mesoscale impacts of wind farms as parameterized in a mesoscale NWP model. *Mon. Wea. Rev.*, **140**, 3017–3038.
- , J. K. Lundquist, and J. B. Olson, 2013: Mesoscale influences of wind farms throughout a diurnal cycle. *Mon. Wea. Rev.*, **141**, 2173–2198.
- Garratt, J. R., 1992: *The Atmospheric Boundary Layer*. Cambridge University Press, 316 pp.
- , 1993: Sensitivity of climate simulations to land-surface and atmospheric boundary-layer treatments—A review. *J. Climate*, **6**, 419–448.
- Hansen, K. S., R. J. Barthelmie, L. E. Jensen, and A. Sommer, 2012: The impact of turbulence intensity and atmospheric stability on power deficits due to wind turbine wakes at Horns Rev wind farm. *Wind Energy*, **15**, 183–196, doi:10.1002/we.512.
- Helmis, C. G., K. H. Papadopoulos, D. N. Asimakopoulos, P. G. Papageorgas, and A. T. Soilemes, 1995: An experimental study of the near-wake structure of a wind turbine operating over complex terrain. *Sol. Energy*, **54**, 413–428, doi:10.1016/0038-092X(95)00009-G.
- Högström, U., D. N. Asimakopoulos, H. Kambezidis, C. G. Helmis, and A. Smedman, 1988: A field study of the wake behind a 2 MW wind turbine. *Atmos. Environ.*, **22**, 803–820.
- Hopwood, W. P., 1995: Surface transfer of heat and momentum over an inhomogeneous vegetated land surface. *Quart. J. Roy. Meteor. Soc.*, **121**, 1549–1574, doi:10.1002/qj.49712152704.
- Ivanova, L. A., and E. D. Nadyozhina, 2000: Numerical simulation of wind farm influence on wind flow. *Wind Eng.*, **24**, 257–269, doi:10.1260/0309524001495620.
- Jensen, L. E., 2007: Analysis of array efficiency at Horns Rev and the effect of atmospheric stability. *Proc. 2007 EWEC Conf.*, Milan, Italy, EWEA.
- Keith, D., J. DeCarolus, D. Denkenberger, D. Lenschow, S. Malyshev, S. Pacala, and P. J. Rasch, 2004: The influence of large-scale wind power on global climate. *Proc. Natl. Acad. Sci. USA*, **101**, 16 115–16 120, doi:10.1073/pnas.0406930101.
- Kirk-Davidoff, D. B., and D. W. Keith, 2008: On the climate impact of surface roughness anomalies. *J. Atmos. Sci.*, **65**, 2215–2234.
- Klemp, J. B., and R. B. Wilhelmson, 1978: The simulation of three-dimensional convective storm dynamics. *J. Atmos. Sci.*, **35**, 1070–1096.
- LeMone, M. A., M. Tewari, F. Chen, J. G. Alfieri, and D. Niyogi, 2008: Evaluation of the Noah land surface model using data from a fair-weather IHOP 2002 day with heterogeneous surface fluxes. *Mon. Wea. Rev.*, **136**, 4915–4941.
- Lenderink, G., and A. A. M. Holtslag, 2000: Evaluation of the kinetic energy approach for modeling turbulent fluxes in stratocumulus. *Mon. Wea. Rev.*, **128**, 244–258.
- Lu, H., and F. Porte-Agel, 2011: Large-eddy simulation of a very large wind farm in a stable atmospheric boundary layer. *Phys. Fluids*, **23**, 065101, doi:10.1063/1.3589857.

- Magnusson, M., and A.-S. Smedman, 1994: Air flow behind wind turbines. *J. Wind Eng. Ind. Aerodyn.*, **80**, 169–189, doi:10.1016/S0167-6105(98)00126-3.
- Mellor, G. L., and T. Yamada, 1982: Development of a turbulence closure model for geophysical fluid problems. *Rev. Geophys.*, **20**, 851–875, doi:10.1029/RG020i004p00851.
- Nakanishi, M., and H. Niino, 2009: Development of an improved turbulence closure model for the atmospheric boundary layer. *J. Meteor. Soc. Japan*, **87**, 895–912, doi:10.2151/jmsj.87.895.
- Poulos, G. S., and Coauthors, 2002: CASES-99: A comprehensive investigation of the stable nocturnal boundary layer. *Bull. Amer. Meteor. Soc.*, **83**, 555–581.
- Rajewski, D., and Coauthors, 2013: Crop Wind Energy Experiment (CWEX): Observations of surface-layer, boundary layer, and mesoscale interactions with a wind farm. *Bull. Amer. Meteor. Soc.*, **94**, 655–672.
- Shin, H., S.-Y. Hong, and J. Dudhia, 2012: Impacts of the lowest model level height on the performance of planetary boundary layer parameterizations. *Mon. Wea. Rev.*, **140**, 664–682.
- Skamarock, W. C., and Coauthors, 2008: A description of the Advanced Research WRF version 3. NCAR Tech. Note NCAR/TN-475+STR, 125 pp.
- Svensson, G., and Coauthors, 2011: Evaluation of the diurnal cycle in the atmospheric boundary layer over land as represented by a variety of single-column models: The second GABLS experiment. *Bound.-Layer Meteor.*, **140**, 177–206, doi:10.1007/s10546-011-9611-7.
- Therry, G., and P. Lacarrere, 1983: Improving the eddy kinetic energy model for planetary boundary layer description. *Bound.-Layer Meteor.*, **25**, 63–88, doi:10.1007/BF00122098.
- Wang, C., and R. G. Prinn, 2010: Potential climatic impacts and reliability of very large-scale wind farms. *Atmos. Chem. Phys.*, **10**, 2053–2061, doi:10.5194/acp-10-2053-2010.
- , and —, 2011: Potential climatic impacts and reliability of large-scale offshore wind farms. *Environ. Res. Lett.*, **6**, 025101, doi:10.1088/1748-9326/6/2/025101.
- Zhou, L., Y. Tian, S. Baidya Roy, C. Thorncroft, L. F. Bosart, and Y. Hu, 2012: Impacts of wind farms on land surface temperature. *Nat. Climate Change*, **2**, 539–543, doi:10.1038/nclimate1505.
- Zilitinkevich, S. S., 1995: Non-local turbulent transport: Pollution dispersion aspects of coherent structure of convective flows. *Air Pollution III*, H. Power, N. Moussiopoulos, and C. A. Brebbia, Eds., Vol. 1, *Air Pollution Theory and Simulation*, Computational Mechanics Publications, 53–60.